iScience

CellPress
OPEN ACCESS

Article

Basal forebrain and prelimbic cortex connectivity is related to behavioral response in an attention task

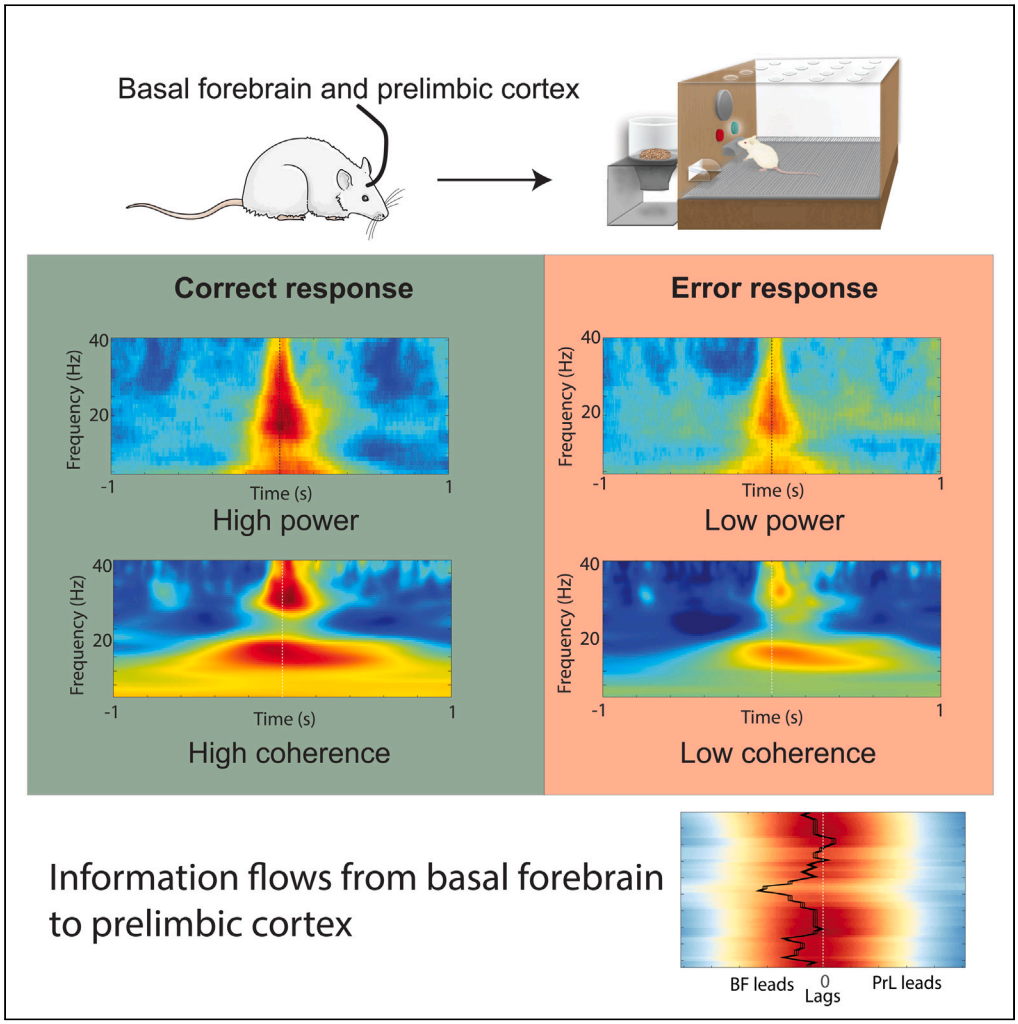

Faezeh Tashakori-Sabzevar, Robert G.K. Munn, David K. Bilkey, Ryan D. Ward

faya.tashakorisabzevar@otago.ac.nz (F.T.-S.)
robert.munn@otago.ac.nz (R.G.K.M.)
ryan.ward@otago.ac.nz (R.D.W.)

Highlights

Spectral power in BF and PrL is higher when correct responses are made

BF and PrL are maximally coherent during correct responses

Information flows from BF to PrL monodirectionally when a correct response is made

Tashakori-Sabzevar et al., iScience 27, 109266
March 15, 2024 © 2024
https://doi.org/10.1016/j.isci.2024.109266

iScience

CellPress
OPEN ACCESS

Article

Basal forebrain and prelimbic cortex connectivity is related to behavioral response in an attention task

Faezeh Tashakori-Sabzevar,[2,4,*] Robert G.K. Munn,[1,4,*] David K. Bilkey,[3] and Ryan D. Ward[3,5,*]

SUMMARY

The basal forebrain (BF) is critical for the motivational recruitment of attention in response to reward-related cues. This finding is consistent with a role for the BF in encoding and transmitting motivational salience and readying prefrontal circuits for further attentional processing. We recorded local field potentials to determine connectivity between prelimbic cortex (PrL) and BF during the modulation of attention by reward-related cues. We find that theta and gamma power are robustly associated with behavior. Power in both bands is significantly lower during trials in which an incorrect behavioral response is made. We find strong coherence during responses that are significantly stronger when a correct response is made. We show that information flow is largely monodirectional from BF to and is strongest when correct responses are made. These experiments demonstrate that connectivity between BF and the PrL increases during periods of increased motivational recruitment of attentional resources.

INTRODUCTION

The basal forebrain (BF), specifically the nucleus basalis, provides significant cholinergic output to both cortical and subcortical regions,[1–3] and is thought to be the most significant source of cholinergic innervation in the mammalian brain.[4] It has been shown to have diverse roles in arousal functions, from the regulation of sleep[5] to reward.[6] BF has also been shown to exert significant control over behavioral initiation, and inhibition[7] and regulation of attention.[8] We have recently demonstrated that BF is critical for the motivational recruitment of attention in response to reward-related cues,[9] consistent with literature showing that the BF is fundamental in encoding and transmitting the motivational salience of reward-related cues.[10–12] How, exactly, this information is relayed and used by other regions in the frontal cortex to guide behavior, however, is less clear.

One candidate region to receive this attentional information related to reward is the prelimbic cortex (PrL). The PrL has long been implicated as a region in control of working memory.[13] The PrL receives monosynaptic projections from the hippocampus,[14] providing a route via which long-term consolidated information could be recalled and held ready for use. Lesions of the PrL selectively impair correct action selection based on changing action-outcome contingencies,[15,16] which has been interpreted as a failure to update information about reward cues held in working memory. DREADD inactivation of PrL attenuates responding in operant tasks[17] in a similar fashion to the pharmacological inactivation of PrL[18,19] These findings are in contrast to those from lesions of the nearby infralimbic cortex, which is thought to control habitual stimulus-response behavior,[20] or, more recently, to flexibly allow switching between habitual behavior and other actions.[21] In terms of attention, PrL has been shown both to direct attention toward predictive cues[21] and to down-regulate attention toward redundant cues.[22] Connections between the BF and the PFC have been shown to be critical for both cue detection and attentional control (see Sarter & Lustig[23] for review).

To examine a putative link between BF and PrL during action selection in an attention task, we used *in vivo* electrophysiological recordings to simultaneously record local field potentials in both BF and PrL during behavior in a task that produces the dynamic modulation of attention in response to motivationally significant cues. Our previous work has demonstrated that both the BF and medial prefrontal cortex, including the PrL, are critical for accurate attentional performance during this task.[9,24] A rich human EEG literature also suggests that theta oscillations are critical for the transmission of information held in working memory,[25–28] and studies in rats have long shown that theta is central to hippocampal spatial memory, but also suggest a role in working memory specifically[29–31] so we anticipated that increased theta power and coherence between BF and PrL would be observed when animals make a response that leads to reward. We further expected that when animals make an error in responding that this will be accompanied by reduced theta power and coherence between these regions. Moreover, we expected that information flow would be directed from BF to PrL.

[1]Department of Anatomy, University of Otago, Dunedin 9054, New Zealand
[2]Department of Pharmacology and Toxicology, University of Otago, Dunedin 9054, New Zealand
[3]Department of Psychology, University of Otago, Dunedin 9054, New Zealand
[4]These authors contributed equally
[5]Lead contact
*Correspondence: faya.tashakorisabzevar@otago.ac.nz (F.T.-S.), robert.munn@otago.ac.nz (R.G.K.M.), ryan.ward@otago.ac.nz (R.D.W.)
https://doi.org/10.1016/j.isci.2024.109266

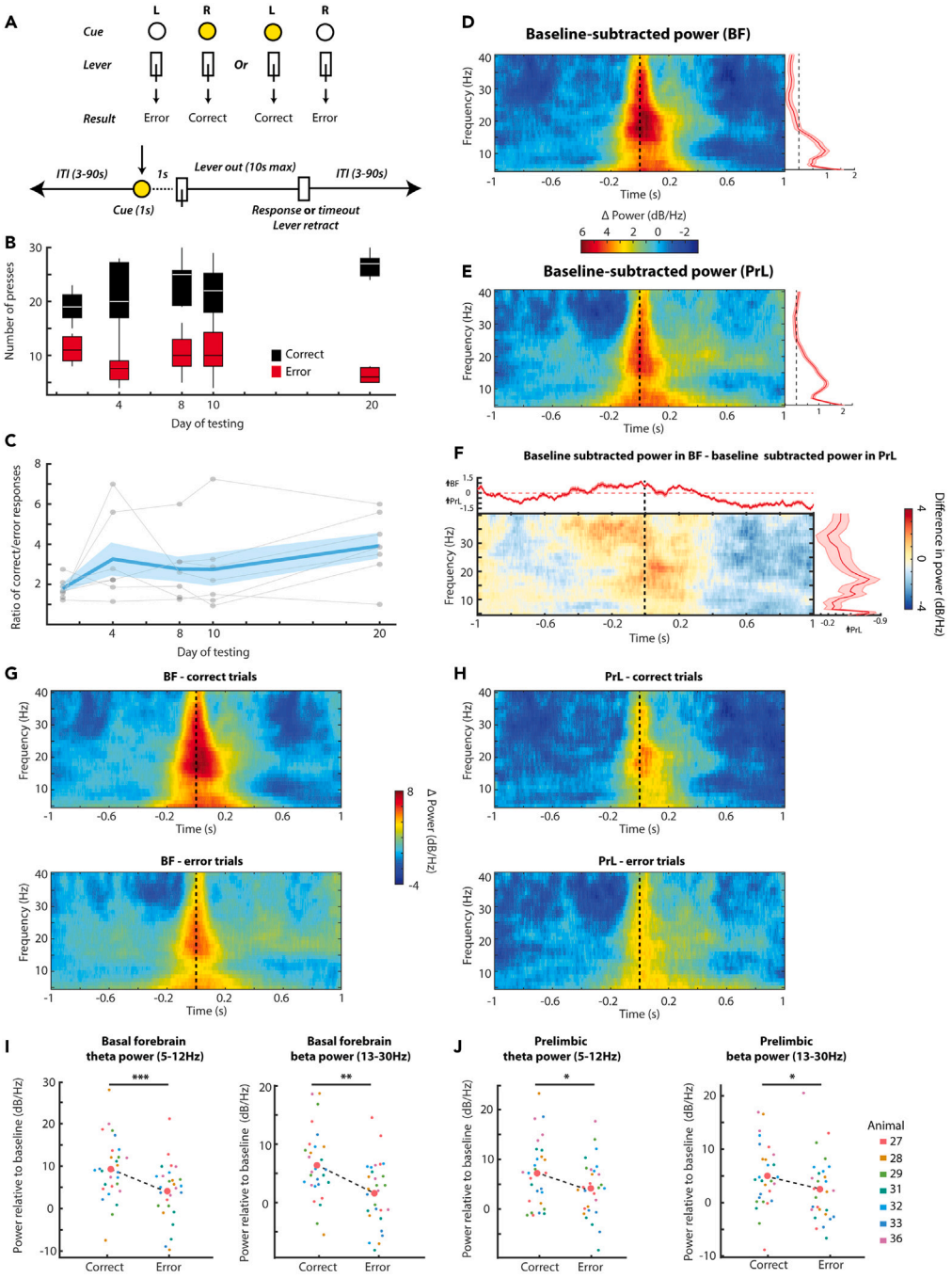

Figure 1. Spectral power in BF and PrL is concentrated around responses and is greater during correct responses than error responses in BF

(A) Schematic illustrating the behavioral task (top) and the timeline of a typical trial (bottom).

(B) Boxplots showing the distribution of correct (black) and error (red) responses on each of days 1, 4, 8, 10 and 20 of testing. The box illustrates the interquartile range and the median.

(C) The ratio (and SEM) of correct responses to error responses over days. The points joined by lines show the ratios of individual animals.

(D and E) The mean baseline-subtracted spectral power (in dB/Hz) in BF (A) and PrL (B) for 2 s around each lever press (vertical black dashed lines). Shaded error bars to the right of each panel show the mean and SEM of power collapsed across time in each region. The vertical line in the attached right-hand panels showing the mean and SEM of power collapsed across time illustrates "0" – the point above which power is greater than the baseline. See also Figure S1 for individual animal data.

Figure 1. *Continued*

(F) The resultant difference in power after subtracting each power spectrum produced from LFP segments recorded from BF from the corresponding spectrum recorded from PrL. Positive values therefore relate to higher power in BF, and negative values correspond to higher power in PrL. Top and right extensions show the mean ± SEM power collapsed across frequency (top) and time (right).

(G and H) Baseline subtracted power over trials in which a correct response was made (top) and an error response was made (bottom) in BF (G) and PrL (H).

(I and J) Scatterplot showing the mean theta (left) and beta (right) power in BF (I) and PrL (J) for each animal in each of the four testing sessions (day 1, 4, 8, and 10) when animals made correct or error responses. Large red dots connected by a black dashed line illustrate the mean over animals and sessions for correct and error responses. (***$p < 0.001$, **$p < 0.01$, *$p < 0.05$).

RESULTS

Animals rapidly make more correct than error responses

Animals (n = 7) consistently made more correct than error responses over training (mean correct responses ±SEM = 21.86 ± 0.95, mean error responses ±SEM = 9.17 ± 0.58, $F(1,68) = 129.11$, $p < 0.001$, Figure 1B) producing a gradually increasing ratio of correct to error responses over training (Figure 1C).

Spectral power in both basal forebrain and prelimbic cortex is concentrated around behavioral responses

We began our analyses of LFP by examining the spectral power in BF and PrL in windows around each lever press. In both BF and PrL, there was a strong increase in power between 5 and 15 Hz that persisted across the peri-response windows, with a peak surrounding the response in each window. To correct for ongoing background activity and isolate changes in power related to each response window, for each 2s section of peri-response LFP, an unrelated epoch of LFP 8 s before each response was identified, and then subtracted from the peri-response epoch. These baseline-subtracted spectra are shown in Figures 1D and 1E and reveal a broadband peak of power in both BF and PrL, lasting for around 350–400 ms and centered on each response. Broad-band power above baseline in BF during the 400 ms around each response was greater than seen in PrL (mean power above baseline −400 ms: 400 ms (dB/Hz) ± SEM; BF = 1.77 ± 0.28, PrL = 1.45 ± 0.23, $t(30) = 6.02$, $p < 0.001$), while power before (mean power above baseline −1000 ms: −400 ms (dB/Hz) ± SEM; BF = −0.54 ± 0.10, PrL = −0.09 ± 0.1, $t(30) = 12.06$, $p < 0.001$) and after this epoch was reduced (mean power above baseline 400 ms: 1000 ms (dB/Hz) ± SEM; BF = −0.82 ± 0.13, PrL = 0.63 ± 0.11, $t(30) = 28.0$, $p < 0.001$, Figure 1F).

Periresponse theta and beta power during correct trials is greater than during error trials in the basal forebrain and prelimbic cortex

We next considered whether there were differences in power in the BF and PrL between trials in which animals made a correct response compared to when they responded in error (Figures 1G and 1H). In general, there was more broad-band power around the response in both regions during the correct trials. We then considered the power in specific frequency bands. In the BF, there was substantially more power in the theta band (5-12 Hz) during correct trials compared to error trials in the 400 ms (−200 to 200 ms) interval around the lever press (mean baseline subtracted theta power ±SEM (dB), correct = 9.29 ± 1.51; error = 4.11 ± 1.10, $F(1,21) = 16.92$, $p < 0.001$) This was also the case in the PrL (mean baseline subtracted theta power ±SEM (dB), correct trials = 7.21 ± 1.14; error trials = 4.17 ± 0.92, $F(1,21) = 6.36$, $p = 0.020$). This pattern was repeated in the beta (13-30 Hz) band; in the BF, correct trials displayed higher power than error trials (mean baseline subtracted beta power ±SEM (dB), correct trials = 6.38 ± 1.24; error trials = 1.59 ± −0.94, $F(1,21) = 13.6$, $p = 0.001$), as did beta power in the PrL (mean baseline subtracted beta power ±SEM (dB), correct trials = 5.02 ± 0.98; error trials = 2.51 ± 1.04, $F(1,21) = 6.32$, $p = 0.020$).

The difference in power between correct and error trials develops and is greater in the basal forebrain than prelimbic cortex

We next sought to determine if the difference in power between correct and error trials varied as a function of the day of testing. Figure 2A shows the power difference between correct and error trials in the basal forebrain for 2 s around each lever press for training days one, four, eight, and ten of training, and this is broken down into mean differences in the theta (5-12 Hz) band, beta (13-30 Hz) band, and gamma (30-120 Hz) bands. Overall, in BF, there was more power across trials across frequency bands (theta, beta, and gamma) during trials in which animals made a correct response compared to error trials (baseline subtracted power (dB) mean ± SEM, correct = 6.10 ± 0.43, error = 3.08, ±1.19. $F(1,6) = 8.250$, $p = 0.028$). This overall difference in power between correct and error trials was true for each frequency band (theta, $t(6) = 2.87$, $p = 0.028$, beta, $t(6) = 2.85$, $p = 0.029$, gamma, $t(6) = 2.86$, $p = 0.029$). Although there appeared to be a peak in power at day 4, there was no significant effect of day ($F(3,18) = 0.432$, $p = 0.732$, n.s.) or interaction between correct/error trials and day of testing ($F(3,18) = 1.206$, $p = 0.336$, n.s.). In PrL, there was an interaction of power in correct/error trials over days of testing (day x correct/error, $F(3,18) = 3.43$, $p = 0.039$). This was driven by power in day one being significantly lower than in day four in the correct trials ($t(6) = 3.08$, $p = 0.022$). The difference between correct and error trials was largest on day 4 across frequency bands but the difference across days was largest in PrL (day x frequency x region, $F(6,36) = 2.370$, $p = 0.049$).

Spectral coherence between basal forebrain and prelimbic cortex is centered on lever press and is lower during error trials

When baseline-subtracted spectral coherence between BF and PrL was calculated, a clear maximum was apparent near the lever press, both when the press was correct (Figure 3A) and, to a lesser degree, when the response was in error (Figure 3B). Broad-band spectral coherence

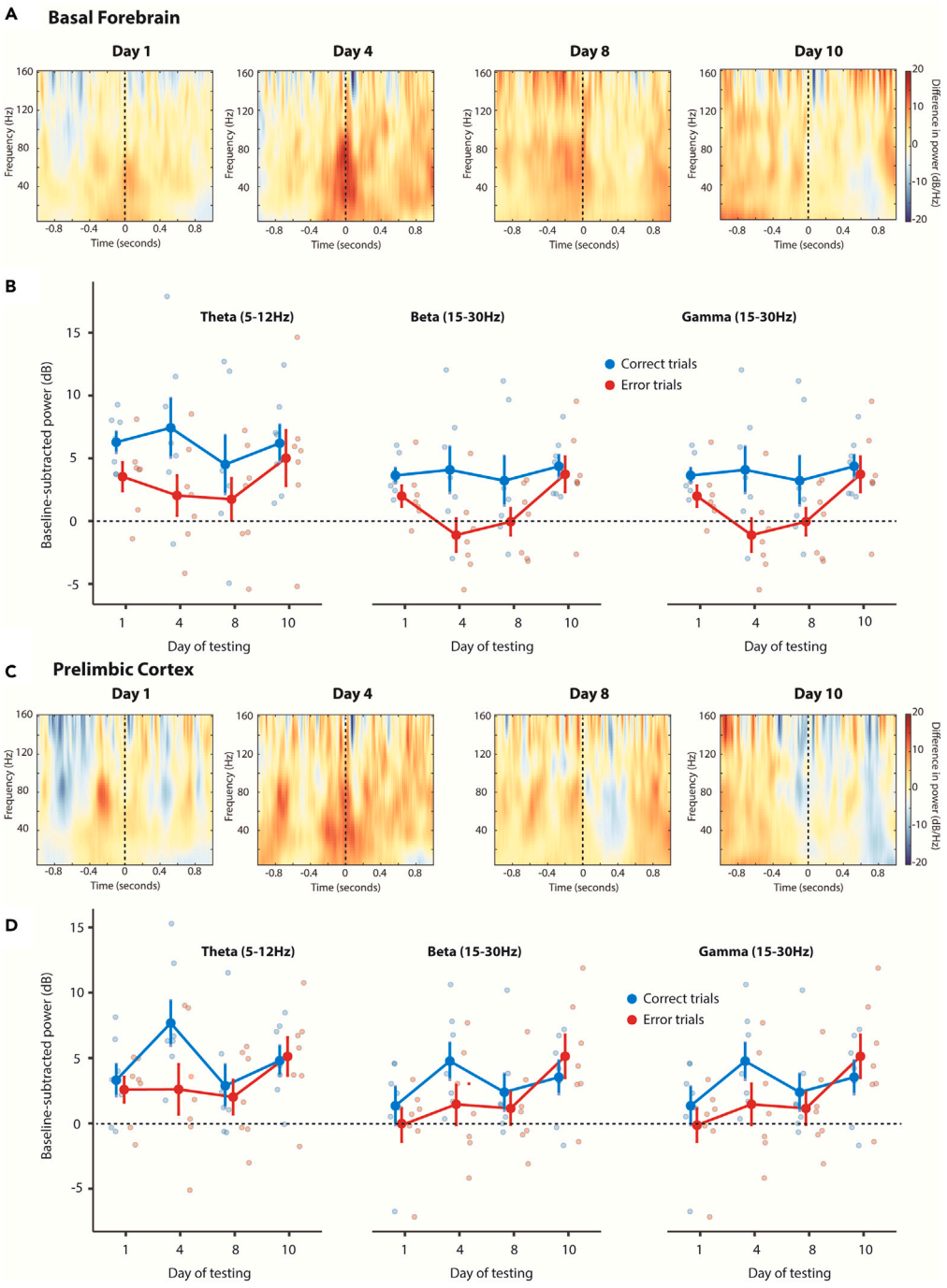

Figure 2. The power difference between correct and error trials changes over days in both BF and PrL

(A) Difference in power between correct and error responses from days (left to right) 1, 4, 8, and 10 of testing. The time of response is illustrated with a black dashed line.

(B) Mean baseline-subtracted power in correct (blue) and error (red) trials during each day of testing in the theta (left), beta (middle), and gamma (right) bands. Individual points are the mean power for each animal over trials within a day. The solid colored lines and dots illustrate the mean values, and the bars at each point are SEM. A black horizontal dashed line shows the transition from more power in the response epoch (positive values) to more power in the baseline (negative values) (C), as in (A), but for recordings from the PrL.

(D) As in (B) but for recordings from PrL.

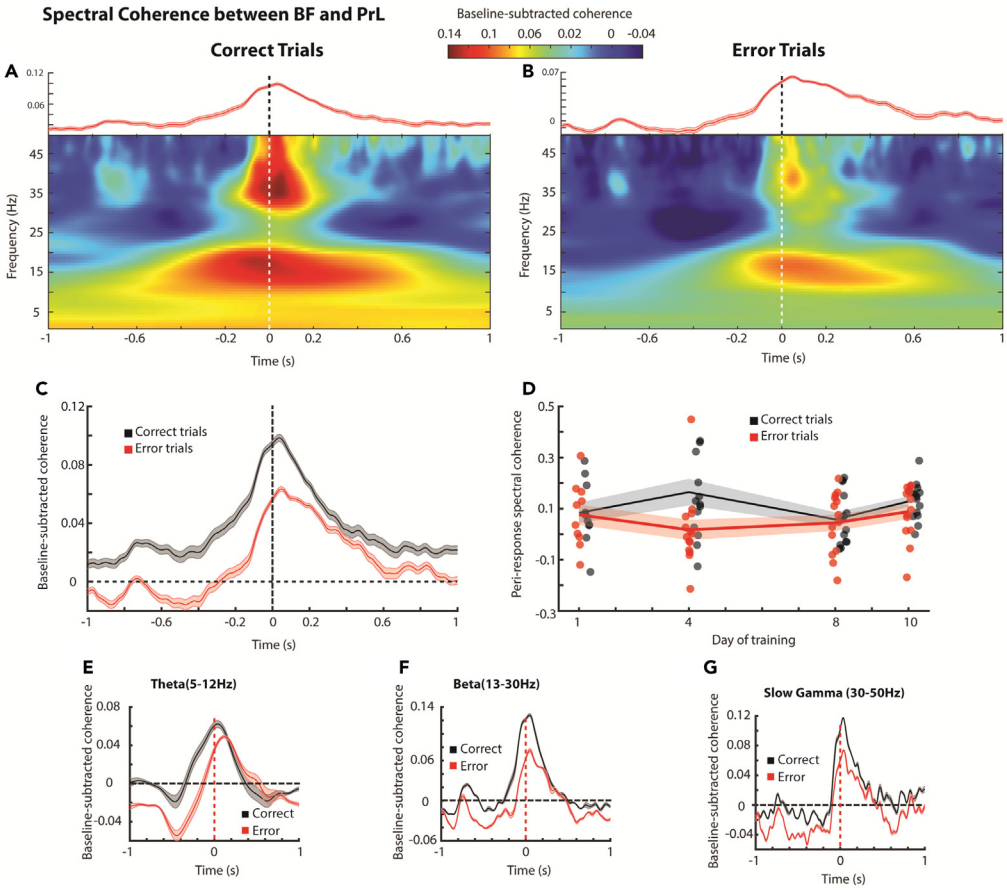

Figure 3. Spectral coherence between BF and PrL is maximal around responses and is greater in correct trials than error trials

(A and B) Mean baseline-subtracted spectral coherence between BF and PrL during trials with correct responses (A) and trials with error responses (B). The time of response in each is marked by a white dashed line. The top panel of each shows the mean ± SEM coherence over time collapsed across frequency.

(C) The mean ± SEM baseline-subtracted coherence for trials in which correct responses were made (black) or error responses were made (red) collapsed across frequency over each response epoch. Black dashed lines indicate the transition from lower than baseline coherence to higher than baseline (horizontal line) and the time of response (vertical line).

(D) Mean peri-response (−100 ms–100ms) spectral coherence between BF and PrL across frequencies on days 1, 3, 8, and 10 of testing. Coherence in correct trials (black) and error trials (red) are shown as an average of all the corresponding trials in each session, with the mean for each day ±SEM shown as shaded lines.

(E–G) As in (C), but for coherence collapsed specifically across the theta (5-12 Hz, E), beta (13-30 Hz, F), and slow gamma (30-50 Hz, G) bands.

was significantly higher during trials in which the correct response was made compared to trials in which an error response was made, and this difference varied over days of testing (day x response, $F(3,18) = 4.196$, $p = 0.020$). This effect was largely driven by the difference in coherence between correct and error trials on day four of testing ($t(6) = 2.63$, $p = 0.039$). In the theta (5-12 Hz) band, the peak of theta appeared to be temporally offset from the lever press, but there was no overall difference in coherence between correct and error trials (response, $F(1,6) = 1.902$, $p = 0.217$, n.s.). In the beta band (15:30 Hz), however, there was a significant difference in coherence between correct and error trials that varied over days of testing (day x response, $F(3,18) = 3.90$, $p = 0.026$). Again, this was largely driven by the difference in coherence between the responses on day 4 ($t(6) = 3.15$, $p = 0.020$). A similar trend was observed in the gamma (30-120 Hz) band, but this effect did not reach significance (day x response, $F(3,18) = 2.844$, $p = 0.067$, n.s.).

Phase of activity during the task

In both the theta (Figure 4A) and beta (Figure 4B) bands, BF and PrL are in phase most strongly at lags during which BF leads PrL slightly (Example theta segment, Figure 4C; mean difference (theta) = −0.988 ms, sign-rank difference from zero test, $Z = 4.61$, $p < 0.001$; mean difference (beta) = −0.48 ms, sign-rank difference from zero test, $Z = 6.06$, $p < 0.001$). There was no change in the resultant vector length that described the magnitude of this offset as the animals proceeded through training.

Previous studies have demonstrated that LFP phase synchronization can occur between regions in conditioning tasks, and that this synchronization can organize local activity.[32–34] When LFP was time-locked to the lever press and averaged across trials, it was apparent that the

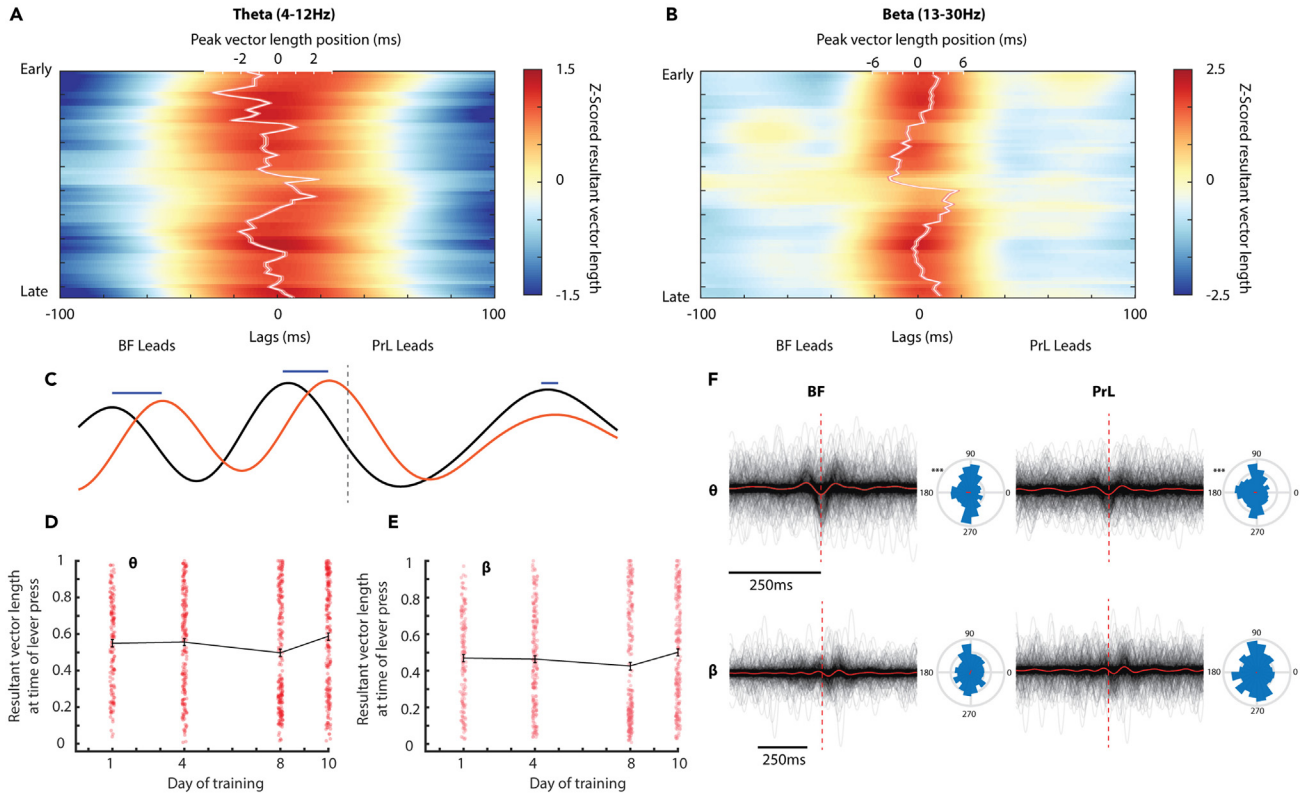

Figure 4. BF phase leads PrL, and is theta phase reset at responding in both the BF and PrL

(A and B) The mean resultant phase vector produced from the phases of LFP bandpassed in the theta (A) and beta (B) bands in BF and PrL, with PrL lagged against BF by −100 ms–100ms. Each row (top to bottom) are single trials from early in training (top) to later in training (bottom). Vector lengths are z-scored in each trial. The white lines indicate the position of the peak in mean vector length in milliseconds. Each panel has been smoothed by rows to aid easy visualization.

(C) An example of theta-band filtered LFP (500 ms of data shown) from BF (black) and PrL (red). Blue lines indicate the peak to peak lead of BF ahead of PrL. The vertical dashed black line denotes the time of response.

(D and E) The peak mean resultant vector for each trial (individual points) bandpassed in the theta (D) and beta (E) bands on days 1, 4, 8, and 10 of training.

(F) Segments of theta (top row) and beta (bottom row) for each response in the BF (left column) and PrL (right column). Solid red lines show the mean phase over all response segments, while the vertical dashed line indicates the time of response. Polar histograms show the distribution of phase angles at the time of response.

lever press tended to occur near the trough of the theta-frequency LFP in both the BF and the PrL (Figure 4F Rayleigh test, BF; $Z = 9.35$, $p < 0.001$, PrL; $Z = 9.57$, $p < 0.001$). The same phase synchrony did not, however, occur in either region in the beta band (Rayleigh test, BF; $Z = 136.65$, $p = 0.1$, n.s., PrL; $Z = 133.50$, $p = 0.50$, n.s.).

Activity in the basal forebrain leads prelimbic cortex in both the theta and beta bands

To examine the directionality of connectivity between BF and PrL during the behavioral task, we first examined lagged cross correlations between segments of LFP from the regions around each response. The mean cross correlation over sessions from early in training to late in training is illustrated in Figures 5A (theta band) and 5B (beta band). Overall, the BF leads the PrL in the theta band (mean peak lag -1 ms, signed rank difference from zero; $Z = 4.61$, $p < 0.001$) and the beta band (mean peak lag −0.45 ms, signed rank difference from zero; $Z = 6.05$ $p < 0.001$). When broken down into correct and error trials, it becomes apparent that BF did not lead PrL in the theta band during correct trials (Figure 5C, mean peak lag = −0.04 ms, signed rank difference from zero; $Z = 0.4$, $p = 0.69$, n.s.). By contrast, BF led PrL in the theta band quite consistently during error trials (mean peak lag = −1.84 ms, signed rank difference from zero; $Z = 4.46$, $p < 0.001$). There was a significant difference in lead/lag between correct and error trials in the theta band ($Z = 4.91$, $p < 0.001$). In the beta band, BF led PrL during both correct and error trials (Figure 5D, correct mean peak lag = −0.47 ms, signed rank difference from zero; $Z = 4.90$, $p < 0.001$; error mean peak lag = −0.40 ms, signed rank difference from zero; $Z = 3.20$, $p = 0.0014$) with no difference between trial type ($Z = 0.82$, $p = 0.41$, n.s.). However, there was a larger lead between BF and PrL during correct trials compared to error trials ($Z = 2.73$, $p = 0.006$). To determine if there was specific directionality between the regions during trials, spectral granger causality was computed between each region for trials in which the correct response occurred and for trials in which error responses occurred (Figures 5E and 5F). During correct trials, granger causality from BF to PrL and from PrL to BF peaked at approximately the time the lever was pressed, although the granger causality in the BF to PrL direction was much higher than the contraflow direction (signed-rank test, $Z = 2.72$, $p = 0.0065$). In both directions, there was lower granger causality when errors

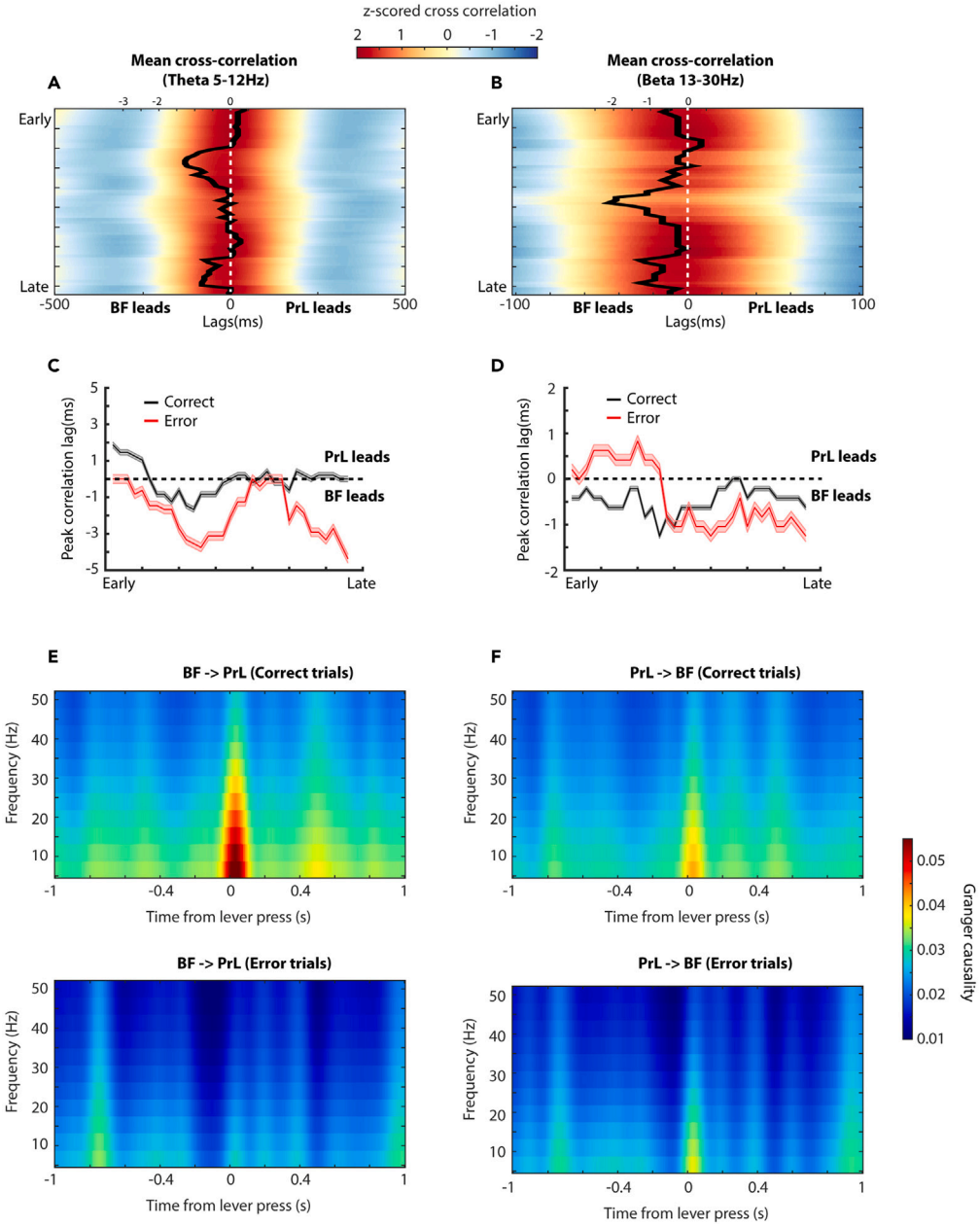

Figure 5. Information flows from BF to PrL during correct but not error trials

(A and B) The mean cross-correlation between BF and PrL for LFP is filtered in the theta (A) and beta (B) bands, as PrL is lagged against the BF by −500 to 500 ms. Data for sessions are stacked vertically from the beginning of testing (top) to the end (bottom). The black lines in each denote the position of the peak correlation over sessions. The extent of the black line shows the SEM for this measure. The vertical white dashed line shows the point of 0 lag between the two LFP segments. Data are z-scored and smoothed vertically for ease of viewing.

(C and D) The time that the peak correlation between BF and PrL occurred in the theta (C) and beta (D) bands as training progressed, split into trials where a correct response was made (black lines) and when an error response was made (red lines). Trials are ordered from "early" to "late" sequentially. The horizontal dashed line denotes the point of 0 lag between regions.

(E) The mean spectral granger causality from BF to PrL from 1 s prior to, to 1 s after each response. The top panel shows granger causality from correct trials, while the bottom shows granger causality for error trials.

(F) As in (E), but showing granger causality from PrL to BF.

were made, but this difference was more pronounced for BF to PrL granger causality than granger causality in the opposite direction. Taken together, these findings suggest a directional flow of information from BF to PrL during responses. Correct responses are associated with a stronger connectivity between BF and PrL, while error responses are associated with overall lower connectivity between the regions. Moreover, the directionality differences demonstrate that it is unlikely that the synchrony between these regions can be explained by volume conduction alone.

DISCUSSION

In these experiments, we demonstrate a striking peri-response increase in theta and beta-band power in both the BF and PrL as animals complete each trial, with the difference in power between correct and error trials being more pronounced on day 4 compared to subsequent days. We also observe that the peri-response power in BF (but not PrL) is lower in these frequency bands during trials in which animals make an error response compared to trials in which they respond correctly. Critically, spectral coherence between BF and PrL is also maximal around each response and is concentrated in the high theta to beta range and the gamma range. Again, we observe relatively high coherence between BF and PrL during trials in which animals made correct responses, while there was relatively less spectral coherence between these structures during error trials. Over several measures, we observe activity in the BF leading the PrL; lagged correlations of segments of LFP showed maximal correlations more often when PrL was advanced relative to BF, suggesting activity in the PrL most resembled activity in BF from several milliseconds prior. Granger causality analysis also suggested robust BF to PrL flow, along with a weaker counterflow from PrL to BF. Of particular note is that the BF to PrL flow was only detected when animals made correct responses; this information transfer appeared to be mostly absent during trials in which animals made error responses. Taken together, these findings are strongly suggestive of information being passed from BF to PrL during an operant attention task requiring action-outcome evaluation, with theta and beta bands being the most prominent contributors to this information transfer. Furthermore, these findings support previous results showing a specific role for the BF cholinergic system in tasks that require the dynamic modulation of attention. Finally, the directionality results suggest that cholinergic input in response to attentional demand is processed by PrL in preparation for optimal responding depending on the task requirements.

The prominence of the theta band in our findings is perhaps not surprising since the BF is home to the major cholinergic output in the mammalian brain and is a driver of the dominant theta rhythm characteristic of the hippocampus and entorhinal cortex. The observation that changes in the beta band are also a central feature of our findings is less expected. Previous work has demonstrated that beta-band oscillations in the BF are associated with object-cued reinforcement learning.[35] Beta-band power during exploration in the hippocampus has also recently been shown to be associated with successful recall.[36] Perhaps of most relevance to our findings, beta power has also been associated with the use of a cue to guide motor output.[37] The peri-response organization of beta power we observe may fulfill a similar function. Beta oscillations have been attributed to cognition and attention, and in PrL they have been shown to be readily induced through cholinergic agonism,[38] suggesting cholinergic output from BF to PrL may drive the transfer of information between these regions. While our data do not explicitly confirm a necessary role for BF-PrL connectivity in the performance of the present experimental task, our prior work indicating a critical role for both the BF and the PrL in this task strongly suggests that this connection is crucial to adaptive performance. Future work is needed to clarify if and how the circuitry and oscillation patterns identified here are required or causal to the outcomes observed. Moreover, while our results suggest an important role for the transfer of information from BF to PrL during reward-motivated attention, recent work has indicated that both the specific character of firing of neural ensembles and location-specific projections from PrL play a dynamic role in the processing of reward-associated cues during learning and in both activating and inhibiting the resulting behavioral outputs.[39,40] It will be important for future work to determine the specific nature and function of downstream signaling from PrL (perhaps to the striatum), which contributes to performance in our task and other paradigms that involve dynamic changes in cue-induced reward-motivated attention and other cognitive processes.

The observation that there was less theta and beta band power during error responses compared to correct responses is largely consistent with previous literature. Esmaeili & Diamond[41] demonstrate significantly fewer units in PrL encoded a tactile discrimination stimulus during error trials compared to trials in which animals made a correct response and were significantly less coherent with theta phase during error trials. In a study examining anterior cingulate and medial prefrontal coordination in Macaques, Voloh et al.[42] demonstrated significant theta/gamma phase amplitude coupling in correct response but not error response trials, along with a similar theta/gamma phase reset related to cue. In humans, a task involving working memory showed higher theta power in the prefrontal cortex during correct trials compared to error trials.[26] The more pronounced difference in power across bands between correct and error responses on day 4 is consistent with an interpretation based on increased attention during the initial exposure to the dynamic modulation of reward probabilities. Previous work has demonstrated increased power in the initial phases of an unpredictable or dynamic learning task, which decreases with increased exposure in both rats[35] and humans[43] Thus, it is possible that the increased differentiation between correct and error responses reflects increased attention to the task during the initial exposure to the dynamic and unpredictably changing reward probabilities.

Limitations of the study

It remains unclear if the changes we observe in power and coherence are the cause of the difference in performance (that is, an error response is produced from a failure to effectively transmit information from working memory to action selection) or whether these changes could be attributed to behavioral changes. For example, it is feasible that error responses result in less robust motor output, resulting in a lever press with less force than a correct trial. Future research combining behavioral tracking and lever force recording could disentangle these possibilities. One further possibility is that the differences in power and coherence are not causative of errors in performance, but reflective of differences in the strength of an input upstream of BF that is instead reflective of the strength of a "certainty" mechanism of an already selected motor program.

STAR★METHODS

Detailed methods are provided in the online version of this paper and include the following:

- KEY RESOURCES TABLE
- RESOURCE AVAILABILITY
  - Lead contact
  - Materials availability
  - Data and code availability
- EXPERIMENTAL MODEL AND STUDY PARTICIPANT DETAILS
- METHOD DETAILS
  - Med-Associates operant chambers
  - Custom-built operant chamber
  - Surgery
  - Behavioral procedures
- QUANTIFICATION AND STATISTICAL ANALYSIS
  - LFP data analysis

SUPPLEMENTAL INFORMATION

Supplemental information can be found online at https://doi.org/10.1016/j.isci.2024.109266.

ACKNOWLEDGMENTS

We thank Sophie French for her exceptional animal care. We acknowledge Richard Hamelink for his assistance in programming the custom operant chamber and Lindsay Robertson for troubleshooting the electrophysiological facilities. Image of operant chamber in graphical abstract from bioicons (http://bioicons.com) by DBCLS and adult rat by Servier modified under a CC-BY license. Funding for these experiments came from performance-based research funding and departmental funds from the University of Otago.

AUTHOR CONTRIBUTIONS

Conceptualization and methodology, R.D.W and D.K.B.; software, R.G.K.M.; formal analysis, R.G.K.M.; investigation, F.T-S.; writing – original draft, F.T-S., R.G.K.M., R.D.W., and D.K.B. Writing – review and editing, F.T-S., R.G.K.M., R.D.W., and D.K.B.; visualization, R.G.K.M.; supervision, R.D.W. and D.K.B.

DECLARATION OF INTERESTS

The authors declare no competing interests.

Received: July 11, 2023
Revised: January 1, 2024
Accepted: February 14, 2024
Published: February 19, 2024

REFERENCES

1. Agostinelli, L.J., Geerling, J.C., and Scammell, T.E. (2019). Basal Forebrain Subcortical Projections. Brain Struct. Funct. *224*, 1097–1117. https://doi.org/10.1007/s00429-018-01820-6.
2. Rye, D.B., Wainer, B.H., Mesulam, M.-M., Mufson, E.J., and Saper, C.B. (1984). Cortical projections arising from the basal forebrain: A study of cholinergic and noncholinergic components employing combined retrograde tracing and immunohistochemical localization of choline acetyltransferase. Neuroscience *13*, 627–643. https://doi.org/10.1016/0306-4522(84)90083-6.
3. Jones, B.E. (2004). Activity, modulation and role of basal forebrain cholinergic neurons innervating the cerebral cortex. In Progress in Brain Research Acetylcholine in the Cerebral Cortex (Elsevier), pp. 157–169. https://doi.org/10.1016/S0079-6123(03)45011-5.
4. Goard, M., and Dan, Y. (2009). Basal Forebrain Activation Enhances Cortical Coding of Natural Scenes. Nat. Neurosci. *12*, 1444–1449. https://doi.org/10.1038/nn.2402.
5. Anaclet, C., Pedersen, N.P., Ferrari, L.L., Venner, A., Bass, C.E., Arrigoni, E., and Fuller, P.M. (2015). Basal forebrain control of wakefulness and cortical rhythms. Nat. Commun. *6*, 8744. https://doi.org/10.1038/ncomms9744.
6. Wilkinson, L.S., Dias, R., Thomas, K.L., Augood, S.J., Everitt, B.J., Robbins, T.W., and Roberts, A.C. (1997). Contrasting effects of excitotoxic lesions of the prefrontal cortex on the behavioural response to d-amphetamine and presynaptic and postsynaptic measures of striatal dopamine function in monkeys. Neuroscience *80*, 717–730. https://doi.org/10.1016/S0306-4522(97)00075-4.
7. Mayse, J.D., Nelson, G.M., Avila, I., Gallagher, M., and Lin, S.-C. (2015). Basal forebrain neuronal inhibition enables rapid behavioral stopping. Nat. Neurosci. *18*, 1501–1508. https://doi.org/10.1038/nn.4110.
8. Voytko, M.L., Olton, D.S., Richardson, R.T., Gorman, L.K., Tobin, J.R., and Price, D.L. (1994). Basal forebrain lesions in monkeys disrupt attention but not learning and memory. J. Neurosci. *14*, 167–186. https://doi.org/10.1523/JNEUROSCI.14-01-00167.1994.
9. Tashakori-Sabzevar, F., and Ward, R.D. (2018). Basal Forebrain Mediates Motivational Recruitment of Attention by Reward-Associated Cues. Front. Neurosci. *12*, 786. https://doi.org/10.3389/fnins.2018.00786.

10. Lin, S.-C., and Nicolelis, M.A.L. (2008). Neuronal ensemble bursting in the basal forebrain encodes salience irrespective of valence. Neuron *59*, 138–149. https://doi.org/10.1016/j.neuron.2008.04.031.
11. Avila, I., and Lin, S.-C. (2014). Distinct neuronal populations in the basal forebrain encode motivational salience and movement. Front. Behav. Neurosci. *8*, 421. https://doi.org/10.3389/fnbeh.2014.00421.
12. Lin, S.-C., Brown, R.E., Hussain Shuler, M.G., Petersen, C.C.H., and Kepecs, A. (2015). Optogenetic Dissection of the Basal Forebrain Neuromodulatory Control of Cortical Activation, Plasticity, and Cognition. J. Neurosci. *35*, 13896–13903. https://doi.org/10.1523/JNEUROSCI.2590-15.2015.
13. Ragozzino, M.E., Detrick, S., and Kesner, R.P. (2002). The Effects of Prelimbic and Infralimbic Lesions on Working Memory for Visual Objects in Rats. Neurobiol. Learn. Mem. *77*, 29–43. https://doi.org/10.1006/nlme.2001.4003.
14. Thierry, A.-M., Gioanni, Y., Dégénétais, E., and Glowinski, J. (2000). Hippocampo-prefrontal cortex pathway: Anatomical and electrophysiological characteristics. Hippocampus *10*, 411–419. https://doi.org/10.1002/1098-1063(2000)10:4<411::AID-HIPO7>3.0.CO;2-A.
15. Corbit, L.H., and Balleine, B.W. (2003). The role of prelimbic cortex in instrumental conditioning. Behav. Brain Res. *146*, 145–157. https://doi.org/10.1016/j.bbr.2003.09.023.
16. Coutureau, E., Marchand, A.R., and Di Scala, G. (2009). Goal-directed responding is sensitive to lesions to the prelimbic cortex or basolateral nucleus of the amygdala but not to their disconnection. Behav. Neurosci. *123*, 448. https://doi.org/10.1037/a0014818.
17. Shipman, M.L., Johnson, G.C., Bouton, M.E., and Green, J.T. (2019). Chemogenetic Silencing of Prelimbic Cortex to Anterior Dorsomedial Striatum Projection Attenuates Operant Responding. eNeuro *6*. ENEURO. 0125, 19.2019. https://doi.org/10.1523/ENEURO.0125-19.2019.
18. Hart, G., Bradfield, L.A., and Balleine, B.W. (2018). Prefrontal Corticostriatal Disconnection Blocks the Acquisition of Goal-Directed Action. J. Neurosci. *38*, 1311–1322. https://doi.org/10.1523/JNEUROSCI.2850-17.2017.
19. Trask, S., Shipman, M.L., Green, J.T., and Bouton, M.E. (2017). Inactivation of the Prelimbic Cortex Attenuates Context-Dependent Operant Responding. J. Neurosci. *37*, 2317–2324. https://doi.org/10.1523/JNEUROSCI.3361-16.2017.
20. Haddon, J.E., and Killcross, S. (2011). Inactivation of the infralimbic prefrontal cortex in rats reduces the influence of inappropriate habitual responding in a response-conflict task. Neuroscience *199*, 205–212. https://doi.org/10.1016/j.neuroscience.2011.09.065.
21. Sharpe, M.J., and Killcross, S. (2015). The prelimbic cortex directs attention toward predictive cues during fear learning. Learn. Mem. *22*, 289–293. https://doi.org/10.1101/lm.038273.115.
22. Sharpe, M.J., and Killcross, S. (2014). The Prelimbic Cortex Contributes to the Down-Regulation of Attention Toward Redundant Cues. Cereb. Cortex *24*, 1066–1074. https://doi.org/10.1093/cercor/bhs393.
23. Sarter, M., and Lustig, C. (2019). Cholinergic double duty: cue detection and attentional control. Curr. Opin. Psychol. *29*, 102–107. https://doi.org/10.1016/j.copsyc.2018.12.026.
24. Kahn, J.B., Ward, R.D., Kahn, L.W., Rudy, N.M., Kandel, E.R., Balsam, P.D., and Simpson, E.H. (2012). Medial prefrontal lesions in mice impair sustained attention but spare maintenance of information in working memory. Learn. Mem. *19*, 513–517. https://doi.org/10.1101/lm.026302.112.
25. Ishii, R., Canuet, L., Ishihara, T., Aoki, Y., Ikeda, S., Hata, M., Katsimichas, T., Gunji, A., Takahashi, H., Nakahachi, T., et al. (2014). Frontal midline theta rhythm and gamma power changes during focused attention on mental calculation: an MEG beamformer analysis. Front. Hum. Neurosci. *8*, 406. https://doi.org/10.3389/fnhum.2014.00406.
26. Itthipuripat, S., Wessel, J.R., and Aron, A.R. (2013). Frontal theta is a signature of successful working memory manipulation. Exp. Brain Res. *224*, 255–262. https://doi.org/10.1007/s00221-012-3305-3.
27. Sauseng, P., Griesmayr, B., Freunberger, R., and Klimesch, W. (2010). Control mechanisms in working memory: A possible function of EEG theta oscillations. Neurosci. Biobehav. Rev. *34*, 1015–1022. https://doi.org/10.1016/j.neubiorev.2009.12.006.
28. Sauseng, P., Klimesch, W., Schabus, M., and Doppelmayr, M. (2005). Fronto-parietal EEG coherence in theta and upper alpha reflect central executive functions of working memory. Int. J. Psychophysiol. *57*, 97–103. https://doi.org/10.1016/j.ijpsycho.2005.03.018.
29. Farrokhi, A., Tafakori, S., and Daliri, M.R. (2022). Dynamic theta-modulated high frequency oscillations in rat medial prefrontal cortex during spatial working memory task. Physiol. Behav. *254*, 113912. https://doi.org/10.1016/j.physbeh.2022.113912.
30. Li, S., Ouyang, M., Liu, T., Bai, W., Yi, H., and Tian, X. (2014). Increase of spike–LFP coordination in rat prefrontal cortex during working memory. Behav. Brain Res. *261*, 297–304. https://doi.org/10.1016/j.bbr.2013.12.030.
31. Li, S., Bai, W., Liu, T., Yi, H., and Tian, X. (2012). Increases of theta–low gamma coupling in rat medial prefrontal cortex during working memory task. Brain Res. Bull. *89*, 115–123. https://doi.org/10.1016/j.brainresbull.2012.07.012.
32. Likhtik, E., Stujenske, J.M., Topiwala, M.A., Harris, A.Z., and Gordon, J.A. (2014). Prefrontal entrainment of amygdala activity signals safety in learned fear and innate anxiety. Nat. Neurosci. *17*, 106–113. https://doi.org/10.1038/nn.3582.
33. Taub, A.H., Perets, R., Kahana, E., and Paz, R. (2018). Oscillations Synchronize Amygdala-to-Prefrontal Primate Circuits during Aversive Learning. Neuron *97*, 291–298.e3. https://doi.org/10.1016/j.neuron.2017.11.042.
34. Karalis, N., Dejean, C., Chaudun, F., Khoder, S., Rozeske, R.R., Wurtz, H., Bagur, S., Benchenane, K., Sirota, A., Courtin, J., and Herry, C. (2016). 4-Hz oscillations synchronize prefrontal–amygdala circuits during fear behavior. Nat. Neurosci. *19*, 605–612. https://doi.org/10.1038/nn.4251.
35. Quinn, L.K., Nitz, D.A., and Chiba, A.A. (2010). Learning-dependent dynamics of beta-frequency oscillations in the basal forebrain of rats. Eur. J. Neurosci. *32*, 1507–1515. https://doi.org/10.1111/j.1460-9568.2010.07422.x.
36. Iwasaki, S., Sasaki, T., and Ikegaya, Y. (2021). Hippocampal beta oscillations predict mouse object-location associative memory performance. Hippocampus *31*, 503–511. https://doi.org/10.1002/hipo.23311.
37. Leventhal, D.K., Gage, G.J., Schmidt, R., Pettibone, J.R., Case, A.C., and Berke, J.D. (2012). Basal Ganglia Beta Oscillations Accompany Cue Utilization. Neuron *73*, 523–536. https://doi.org/10.1016/j.neuron.2011.11.032.
38. van Aerde, K.I., Heistek, T.S., and Mansvelder, H.D. (2008). Prelimbic and Infralimbic Prefrontal Cortex Interact during Fast Network Oscillations. PLoS One *3*, e2725. https://doi.org/10.1371/journal.pone.0002725.
39. Lachaux, J.-P., Rodriguez, E., Martinerie, J., and Varela, F.J. (1999). Measuring phase synchrony in brain signals. Hum. Brain Mapp. *8*, 194–208. https://doi.org/10.1002/(SICI)1097-0193(1999)8:4<194::AID-HBM4>3.0.CO;2-C.
40. Protopapa, F., Siettos, C.I., Evdokimidis, I., and Smyrnis, N. (2014). Granger causality analysis reveals distinct spatio-temporal connectivity patterns in motor and perceptual visuo-spatial working memory. Front. Comput. Neurosci. *8*, 146. https://doi.org/10.3389/fncom.2014.00146.
41. Esmaeili, V., and Diamond, M.E. (2019). Neuronal Correlates of Tactile Working Memory in Prefrontal and Vibrissal Somatosensory Cortex. Cell Rep. *27*, 3167–3181.e5. https://doi.org/10.1016/j.celrep.2019.05.034.
42. Voloh, B., Valiante, T.A., Everling, S., and Womelsdorf, T. (2015). Theta–gamma coordination between anterior cingulate and prefrontal cortex indexes correct attention shifts. Proc. Natl. Acad. Sci. USA *112*, 8457–8462. https://doi.org/10.1073/pnas.1500438112.
43. Huycke, P., Verbeke, P., Boehler, C.N., and Verguts, T. (2021). Theta and alpha power across fast and slow timescales in cognitive control. Eur. J. Neurosci. *54*, 4581–4594. https://doi.org/10.1111/ejn.15320.
44. Berens, P. (2009). CircStat: a MATLAB toolbox for circular statistics.
45. Morf, M., Vieira, A., L Lee, D.T., Kailath, T., and Kailath, T. (1978). Recursive Multichannel Maximum Entropy Spectral Estimation. IEEE Trans. Geosci. Electron. *16*, 85–94. https://doi.org/10.1109/TGE.1978.294569.

STAR★METHODS

KEY RESOURCES TABLE

REAGENT or RESOURCE	SOURCE	IDENTIFIER
Experimental models: Organisms/stains		
Subjects: Sprague Dawley	University of Otago Hercus-Taieri Resource Unit	N/A
Software and algorithms		
MATLAB	version 2022a Mathworks	https://www.mathworks.com
Signal Processing Toolbox	Mathworks (2023)	https://au.mathworks.com/help/signal/index.html?s_tid=CRUX_topnav
Circular Statistics Toolbox	Philipp Berens(2023)	https://www.mathworks.com/matlabcentral/fileexchange/10676- circular-statistics-toolbox-directional-statistics

RESOURCE AVAILABILITY

Lead contact

Further information and requests for resources and reagents should be directed to and will be fulfilled by Ryan Ward (ryan.ward@otago.ac.nz).

Materials availability

This paper does not report any unique reagents or engineered organisms.

Data and code availability

- This paper does not report any standardized data.
- Data reported in the paper will be shared with other investigators upon request to the lead contact
- Any additional information or code required to reanalyze the data reported in this paper is available from the lead contact upon request.

EXPERIMENTAL MODEL AND STUDY PARTICIPANT DETAILS

All experimental procedures were reviewed and approved by the University of Otago Animal Welfare Office and conducted in accordance with New Zealand animal welfare legislation (under ethics approval code AUP-49-14). Seven male Long Evans rats (obtained from the University of Otago's Hercus-Taieri Resource Unit) aged between 3 and 4 months old and weighing between 350 and 450 g were used in this study. The animal housing room temperature was kept between 21°C and 23°C and the light maintained on a 12-h, light-dark (6 a.m.–6 p.m.) cycle. All experimentation and training occurred during the 12-h light phase. For two weeks after their arrival, rats were given daily handling, regularly weighing, and free access to water and food pellets. After those free-feeding periods, they were food-deprived of standard rat chow to no less than 85% of their free-feeding weight to motivate them during test phases. They continued to have *ad libitum* access to water. Sweetened condensed milk was used throughout the training as a reward in the operant chambers.

METHOD DETAILS

Med-Associates operant chambers

Eight identical operant chambers (controlled through Med-Associates, St. Albans, VT: model ENV-008w) were used for the preliminary training of the rats. Each operant box was equipped with cue lights above each of two levers, house light and a liquid dipper. Each operant chamber was housed in a light and sound-attenuating chamber. Experimental events were controlled, and data recorded using a dedicated computer running MedPC IV programs and software.

Custom-built operant chamber

A custom-built operant box (with internal dimensions of 24.5 cm length × 24.5 cm width × 23.0 cm height) controlled through an Arduino LLC, Somerville, MA, USA microcontroller, was used for the electrophysiology recording procedure during the behavioral task. The grid floor,

ceiling, the walls, and the waste pan were constructed of stainless steel while the hinged door was made from clear polycarbonate. The operant box was equipped with two levers situated under cue lights, a house light, and a sipper tube. A fixed reward (0.5 mL of condensed milk) was delivered through a sipper tube dispensed condensed milk. The delivery procedure was controlled by a custom-built peristaltic pump (Adafruit, New York, NY, USA) which was placed outside of the chamber to reduce noise and interference during the recording. A sipper tube was used to deliver reward and was flanked by a nose poke feeder door, which was activated when the rats placed their head in the feeder hole. The chamber was placed inside a light and sound-attenuating cabinet. The holes on top of the operant chamber and the external cabinet allowed us to attach the cable through which electrophysiological signals were passed to connect to the rat's head and did not impede the rat's movement. All experimental procedures were controlled and recorded using a dedicated computer running the dacq USB multichannel recording system (Axona Ltd) (which was used for recording local field potentials).

Surgery

A custom-built electrode assembly was used for local field potential recording. Each implanted electrode group consisted of a ground, a reference and two LFP wires. The tip of the LFP electrodes was freshly cut before implantation. All stereotaxic surgeries were performed under aseptic conditions and conducted in accordance with animal care guidelines. Each animal was anesthetized with isoflurane (4–5% induction, 1–2% maintenance) and stereotaxically implanted in the BF (AP: 0.6 mm, ML: 2.25 mm, DV: −7.6 mm from the dura) and PrL (AP: 3 mm, ML: 0.8 mm, DV: -3 mm from the dura) with a non-moveable 75 μm diameter, Teflon coated insulated stainless-steel wire. BF coordinates were adapted from Paxinos & Watson, (2007). Wires were led to a connector that was fastened to the rat's skull with screws and acrylic dental cement.

Rats were given one-week recovery time following surgery, and they were housed individually in their cages with *ad libitum* access to food and water. After that period, food intake was decreased to maintain the rats' weight at 85%–90% of their free-feeding weight to optimize the behavior of the rats during the experiment. The rats were kept under food deprivation during the experiment. Once the rat's weights reached 85%–90% of their base weight behavioral training commenced.

Behavioral procedures

On two consecutive days before training began, rats were given 0.5 mL condensed milk in their home cages. On the following day, rats were trained to consume condensed milk. Rats were first taught to press the lever for a reward. In these sessions, either a left or right lever press resulted in reward delivery. In the next session (single cue-single lever training) the cue light above either the left or right lever was illuminated, and rats were required to press the cued lever for reward. Following the third day of single cue-single lever training in which all rats pressed the cued lever on at least 65 out of 68 trials, the choice training sessions were initiated.

In choice-training, either the left or right lever was cued for 5s. A response on to the cued lever was rewarded. Rats received three sessions each of 50, 75, and 100% choice trials, the remaining trials were single-cue single-lever as described above. During this training phase, incorrect responses initiated a correction procedure in which the trial was repeated with the same cue location until it was completed correctly. Next, rats received three sessions of 100% choice trials with no correction. The cue duration was then reduced from 5s to 1s over the course of 7 sessions. All the above trials took place in the Med-Associates Inc. operant chambers. When all rats were responding correctly on 95% of trials, the custom-build operant chamber was introduced to rats for the recording phase of the study. The number of trials was reduced to 36 during this phase of the study, and the mean intertrial interval was decreased from 45s to 20s (range 3s–90s). The probability of reward for the correct response was signaled the house light (on = 1.0, off = 0.1) for the duration of each trial. The local field potential was recorded simultaneously from the target areas on the first, fourth, eight, tenth and last session (session twenty). A schematic of the behavioral task is shown in Figure 1.

QUANTIFICATION AND STATISTICAL ANALYSIS

LFP data analysis

Data were analyzed in MATLAB (version 2022a, Mathworks, MA) using a combination of custom-written scripts. Some functions relied on the Signal Processing Toolbox and the Circular Statistics Toolbox.[44] LFP power across frequencies was computed using a continuous wavelet transform of the unfiltered LFP signals in 2.5-second-long windows around each response. The wavelet transform was accomplished using the cwt function from the Signal Processing Toolbox in MATLAB using a morse wavelet with symmetry 3 and a time-bandwidth parameter of 60. Baseline subtraction was performed for each LFP window associated with each lever press by selecting a 2.5 s period of LFP 20 s prior to each response as a "baseline". Power in the baseline period was determined as for the period of interest and the power in the baseline period was subtracted from the corresponding period of interest. Coherence between channels was computed as the magnitude-squared wavelet coherence using the function wcoherence from the Signal Processing Toolbox in MATLAB using 12 voices per octave.

Phase synchrony between LFP streams was determined by bandpass filtering the LFP at theta (5-12 Hz) beta (3-30 Hz) and gamma (25-50 Hz) frequencies and obtaining phase information of the Hilbert-transformed signals using the hilbert and angle functions. Phase-phase locking was computed as the mean resultant length (MRL) as

$$\frac{1}{N}\sum_{n=1}^{N}\left|exp\left(j\theta(t,n)\right)\right|$$

Where $\theta(t,n)$ is the difference in phases between the signals ($\varphi 1(t,n) - \varphi 2(t,n)$) after Lachaux et al.[39] The resultant MRL values therefore took on values from 0 (no locking) to 1 (perfect locking). Directionality was computed as a function of lag between BF and PrL LFP from −100 to 100 ms centered around each response. Correlation between the filtered streams of LFP was calculated using the xcorr function in MATLAB. The signals were normalized such that the autocorrelations at 0 lags were set at 1. This was computed for lags from −500 to 500 ms centered on each response.

To further determine directionality, we computed spectral granger causality between the signals. Spectral granger causality was computed in a similar manner to Protopapa et al.[40] Briefly, data were temporally downsampled from 4800 to 225 Hz, using a time window of 400 ms and an order of 15. Stationarity between the signals was improved through subtraction of the ERP for all segments of LFP. Autoregressive models using the LWR method[45] were fit to each channel of LFP and to the joint data. Granger causality between signals x and y at each frequency was calculated by the equation

$$GC_{y\rightarrow x}(\omega) = ln\left(1 + \frac{H_{xy}(\omega)\sigma_{yy}H^{*}_{xy}(\omega)}{H_{xx}(\omega)\sigma_{xx}H^{*}_{xx}(\omega)}\right.$$

Where H is the inverse of the transfer matrix of the model coefficients and σ_{xx} and σ_{yy} are the diagonal elements of the covariance matrix of residuals. This was computed for each time window for each frequency.

All data was interrogated for parametricity using an Anderson-Darling test (results not shown). If data conformed to normality, they were compared using either repeated-measures ANOVA followed by Tukey post-hoc comparisons or a two-tailed t-test where appropriate. Nonparametric data were compared using a Wilcoxon signed-rank test. Angular data was tested for phase clustering using a Rayleigh's test. All analyses used $\alpha = 0.05$.